INTERNATIONAL JOURNAL FOR NUMERICAL METHODS IN FLUIDS
Int. J. Numer. Meth. Fluids **28**: 1481–1501 (1998)

WALL BOUNDARY CONDITIONS FOR INVISCID COMPRESSIBLE FLOWS ON UNSTRUCTURED MESHES

N. BALAKRISHNAN AND G. FERNANDEZ*
Laboratoire SINUMEF, ENSAM, 151, Bd. de l'Hôpital, 75013 Paris, France

SUMMARY

In this paper we revisit the problem of implementing wall boundary conditions for the Euler equations of gas dynamics in the context of unstructured meshes. Both (a) strong formulation, where the zero normal velocity on the wall is enforced explicitly and (b) weak formulation, where the zero normal velocity on the wall is enforced through the flux function are discussed. Taking advantage of both approaches, mixed procedures are defined. The new wall boundary treatments are accurate and can be applied to any approximate Riemann solver. Numerical comparisons for various flow regimes, from subsonic to supersonic, and for various approximate Riemann solvers point out that the mixed boundary procedures drastically improve the accuracy. © 1998 John Wiley & Sons, Ltd.

KEY WORDS: unstructured meshes; wall boundary conditions; aerodynamic; finite volume; upwind scheme; Crocco's relation

1. INTRODUCTION

Accurate calculation of global coefficients, such as lift or drag, are very important for the aerodynamic design of aircrafts and space vehicles. These quantities depend not only on the accuracy of the scheme used for interior nodes, but also on the wall boundary treatment. Various ways of implementing the wall boundary condition to numerically obtain the solution to Euler equations of gas dynamics on structured meshes have been studied extensively [1]. Although the implementation of the wall boundary condition on unstructured meshes involves the extension of ideas which are already known in the context of structured meshes, it is not trivial and often not stated explicitly. Therefore, we re-examine the problem for unstructured meshes for both cell vertex and cell center finite volume schemes.

The satisfaction of the wall boundary condition for the compressible inviscid flows can be achieved using two types of formulations, namely, (a) the strong formulation and (b) the weak formulation. In the strong formulation the values of the state variables on the wall boundary are defined using certain physical constraints. In the weak formulation the values of the state variables on the wall boundary are updated in a way similar to the procedure used for updating the interior cells/nodes. The former is very useful for Taylor Galerkin implicit schemes and for gridless schemes based on the method of least squares for the discretization of the spatial derivatives [2,3]. In this work we investigate both of these formulations of implementing the wall boundary conditions on unstructured meshes, particularly in the context of upwind schemes widely used in industry.

* Correspondence to: Laboratoire SINUMEF, ENSAM, 151 Bd. de l'Hôpital, 75013 Paris, France.

CCC 0271–2091/98/201481–21$17.50

Received May 1996
Revised January 1998

The rest of the paper is organised as follows. The general framework of higher order finite volume schemes on unstructured meshes is presented in Section 2. Various types of wall boundary condition are described in Section 3. The results obtained using different wall boundary conditions in the framework of cell vertex finite volume schemes are presented in Section 4. Concluding remarks are made in Section 5.

2. HIGH ORDER FINITE VOLUME SCHEMES

Using the Gauss theorem, the state update formula for a finite volume scheme is written as

$$\left(\frac{\partial \mathbf{W}_i}{\partial t}\right) = \frac{1}{\Omega_i} \int_{\partial \Omega_i} \mathbf{F}_\perp(\mathbf{W}(\vec{r}, t))\, \mathrm{d}s, \tag{1}$$

where the vector of state variables $\mathbf{W} = (\rho, \rho\vec{u}, E)^T$ represents the mass density, momentum components and total energy. The subscript i represents the values in the ith finite volume Ω_i. The Euler flux normal to the finite volume interface $\partial\Omega_i$ is given by: $\mathbf{F}_\perp = \mathbf{F} \cdot \hat{n} = (\rho u_\perp, \rho u_\perp \vec{u} + p\hat{n}, (E+p)u_\perp)^T$, where $\hat{n}$ is the outward unit normal, $u_\perp = \vec{u} \cdot \hat{n}$ and $u_\parallel = \vec{u} \wedge \hat{n}$ are the normal and tangential velocities to the interface. The pressure p is given by $p = (\gamma - 1)(E - \frac{1}{2}\rho(u_\perp^2 + u_\parallel^2))$, where $\gamma = 1.4$ is the specific heat ratio.

On unstructured meshes it is possible to build finite volume schemes either in cell vertex or cell center framework. Typical cell vertex and cell center finite volumes on a triangulated domain are shown in Scheme 1.

In a cell vertex finite volume framework the state variables are updated at the nodes, whereas in the cell center finite volume framework the state variables are updated at the centroids of the cells. We shall refer to these points in a finite volume as the *reference points*.

For steady state computations. the accurate calculation of fluxes on the cell interface using high order spatial accurate schemes is very important and the time integration can be performed using either implicit or multistage schemes. To achieve high-order spatial accuracy, the method of reconstruction discussed by Barth and Frederickson [4] or Fezoui and Stoufflet [5] is employed. These works can be considered as a multidimensional generalisation of the high-order schemes developed by van Leer [6]. In these procedures the spatial variation of any variable ϕ over a finite volume is represented as

$$\phi(\vec{r}_i + \vec{dr}) = \phi(\vec{r}_i) + (\nabla\phi)_i \cdot \vec{dr}, \tag{2}$$

where $\phi(\vec{r}_i)$ represents the values at the reference points obtained using the state update formula. The variable ϕ used in the above expression is general and can represent conservative, primitive or characteristic variables. The use of variables other than the conservative variable

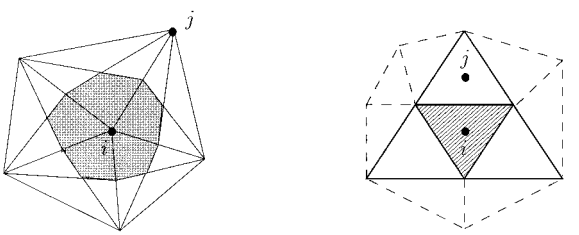

(a) Cell vertex framework (b) Cell center framework

Scheme 1. Control volumes Ω_i.

in the reconstruction procedure is valid when one is interested only in the steady state values. The gradient terms appearing in Equation (2) can be computed in many different ways. In the numerical experiments presented in this paper, the primitive variables are reconstructed and the gradients are obtained using one of the following methods.

2.1. Averaging the gradients in the neighbouring cells

This method of determining the gradients is inspired by the finite element methodology. Linear test functions N are introduced on each triangle to approximate the variable and its gradient on the triangle, such that

$$\phi(\vec{r}) \approx \sum_l \phi_l N_l(\vec{r}),$$

and

$$\nabla\phi\big|_\tau \approx \sum_l \phi_l \nabla N_l.$$

The gradient at vertex i is then recovered using area averaging over the triangles τ sharing the vertex i:

$$\nabla\phi_i = \frac{1}{\sum_{\tau|i\in\tau} \Omega_\tau} \sum_{\tau|i\in\tau} \nabla\phi\big|_\tau \Omega_\tau. \tag{3}$$

This method applies only in a cell vertex framework and we present the next approach which is more general.

2.2. The method of least squares

Here the gradient terms appearing in Equation (2) are obtained by minimising the sum of the squares of the errors [3,7], defined by

$$E_i = \sum_{j=1}^{J} (\Delta\phi_j - (\nabla\phi)_i \cdot \Delta\vec{r}_j)^2, \tag{4}$$

where subscript j represents the neighbouring grid points, J is the number of support points, ϕ_i is the value obtained from the state update formula, $\Delta\phi_j = \phi_j - \phi_i$ and $\Delta\vec{r}_j = \vec{r}_j - \vec{r}_i$. For a linear reconstruction procedure it is possible to obtain a closed form expression for the gradient terms by minimising Equation (4); they are given by

$$\phi_{i,x} = \frac{\|\Delta y\|^2(\Delta x, \Delta\phi) - (\Delta x, \Delta y)\,(\Delta y, \Delta\phi)}{\|\Delta x\|^2\|\Delta y\|^2 - (\Delta x, \Delta y)^2}, \tag{5a}$$

$$\phi_{i,y} = \frac{\|\Delta x\|^2(\Delta y, \Delta\phi) - (\Delta x, \Delta y)(\Delta x, \Delta\phi)}{\|\Delta x\|^2\|\Delta y\|^2 - (\Delta x, \Delta y)^2}, \tag{5b}$$

where

$$\|\Delta x\|^2 = \sum_{j=1}^{N} \Delta x_j^2, \qquad \|\Delta y\|^2 = \sum_{j=1}^{N} \Delta y_j^2,$$

$$(\Delta x, \Delta\phi) = \sum_{j=1}^{N} \Delta x_j\,\Delta\phi_j \quad \text{and} \quad (\Delta y, \Delta\phi) = \sum_{j=1}^{N} \Delta y_j\,\Delta\phi_j.$$

Equations (3) and (5) are used for the determination of the gradients of the variables and are very useful in satisfying gradient boundary conditions on unstructured meshes.

The next step is the calculation of the fluxes at the cell interfaces and they are obtained in the present work using the Roe [8], van Leer [9] and KFVS [10] approximate Riemann solver. The flux formulas of the above mentioned schemes are presented in Appendix A. For linear reconstruction procedure it is sufficient to use a one-point quadrature formula to integrate the fluxes on the interface. The high resolution schemes thus obtained are not monotonicity preserving. Therefore, it becomes necessary to limit the gradients to enforce monotonicity. In the present work we either use the multidimensional limiter developed by Venkatakrishnan [11,18] or a modified minmod limiter.

An important distinction between the two finite volume frameworks discussed earlier, is that the reference points of the boundary cells fall on the boundary in the case of cell vertex schemes and it is not so in the case of cell center schemes. This feature becomes important in enforcing wall boundary conditions, as will be discussed in the following sections.

3. WALL BOUNDARY CONDITIONS

For a solid wall only one characteristic enters the flow domain and it is necessary to provide only one fact on the wall based on physical considerations (natural boundary condition, $u_\perp = 0$). The remaining information for defining the state variables on the wall must be derived from within the flow domain (numerical boundary condition). Thus, when enforcing zero mass flux on the body, the flux formula for a stationary wall reduces to

$$\mathbf{F}_{\perp \mathrm{B}} = p_{\mathrm{B}} \begin{bmatrix} 0 \\ n_x \\ n_y \\ 0 \end{bmatrix} . \tag{6}$$

As mentioned earlier, the wall boundary condition can be satisfied either using strong formulation or using weak formulation. These formulations differ in the way the state variables are updated in the boundary cells. In the following section we present the strong formulation in greater detail, the use of which is not so common in the framework of unstructured meshes. Then, some of the conventional weak formulations, followed by three modified weak formulations are presented.

3.1. Strong formulation

In the strong formulation the state variables are updated at all the interior nodes using the state update formula (1). Then, the state variables on the boundary are updated using the new information available in the interior nodes with the following physical constraints:

$$u_\perp = 0, \tag{7a}$$

$$\frac{\partial S}{\partial n} = -\frac{\gamma - 1}{\rho^{\gamma - 1}} u_\parallel \omega, \tag{7b}$$

$$\frac{\partial H}{\partial n} = 0, \tag{7c}$$

$$\frac{\partial p}{\partial n} = -\rho \frac{u_{\parallel}^2}{\mathscr{R}}. \tag{7d}$$

In the above expression $S = p/\rho^{\gamma}$ is an entropy-like variable, $H = (E+p)/\rho$ is the total enthalpy, ω is the vorticity, $\mathscr{R}$ is the radius of curvature of the wall boundary and n represents the direction normal to the wall. The value of any variable ϕ (S, H or p as the case may be) on the wall can be obtained by enforcing the conditions on the normal gradients using Equations (3) or (5).

Equation (7b) is simply the Crocco's relation [12] in a direction normal to the wall, wherein the isenthalpy of the flow is assumed. In the case of inviscid subsonic flows without discontinuities, this relation becomes

$$\frac{\partial S}{\partial n} = 0. \tag{8}$$

Enforcing zero normal entropy gradient on the wall boundary has been found to be less dissipative for subsonic flows and transonic flows. In most of the computations presented in this paper constraint (8) is used in preference to Equation (7b), except when otherwise mentioned. This aspect will be discussed in greater detail in Section 4. The total enthalpy remains constant for inviscid flows without source terms if the flow at infinity is isenthalpic. Therefore, Equation (7c) is also a valid boundary condition and is used to obtain $u_{\parallel}$.

Equation (7d) corresponds to the normal momentum equation for rigid stationary walls satisfying $\partial u_{\perp}/\partial t = 0$. The use of the radius of curvature in satisfying normal momentum equation can be avoided simply by using the differential relation obtained from the non-conservative form of the Euler equations:

$$\frac{\partial p}{\partial n} = -p\hat{n} \cdot ((\vec{u} \cdot \nabla)\vec{u}). \tag{9}$$

It is possible to obtain a similar relation for the normal gradient of pressure on the wall using the conservative form of the Euler equations. Yet another way of determining the pressure on the wall satisfying the normal momentum equation is to use the conservative integral relation [13]:

$$\int_{\partial\Omega_B} \mathbf{F}_{\perp}\, \mathrm{d}s = -\int_{\partial\Omega_I} \mathbf{F}_{\perp}\, \mathrm{d}s.$$

In the above equation $\partial\Omega_B$ and $\partial\Omega_I$ represent the boundary and the interior edges of a wall boundary cell respectively. Assuming that the pressure is constant along the boundary edges of each of the wall boundary cells, the relation for the pressure on the boundary is

$$p_B = -\frac{1}{\Delta s_B}\left[n_x \int_{\partial\Omega_I} F_{\perp 2}\, \mathrm{d}s + n_y \int_{\partial\Omega_I} F_{\perp 3}\, \mathrm{d}s\right], \tag{10}$$

where Δs_B is the length of the boundary edge. In this work we adopt either Equation (9) or (10) to satisfy the normal momentum equation on the wall. Therefore, based on the way the normal momentum equation is satisfied, we have two variations of implementing the strong boundary condition. In the variation *Method Sa* the wall pressures are determined using the differential relation (9), whereas in *Method Sb* they are determined using the conservative integral relation (10).

When the flow is irrotational (i.e. when Equation (8) is a valid approximation), we have

$$\omega = 0. \tag{11}$$

The above relation is used to obtain $u_{\|}$. This leads us to the third variation of the strong boundary condition, *Method Sc*, wherein the constraint on the normal enthalpy (7c) is replaced by Equation (11).

The main advantage of the strong formulation is that it is less dissipative and takes into account the effect of curvature of the wall boundary. The curvature effects are present in Equation (7d). They also arise in Equation (7b) through the vorticity, rewritten as $\omega = (u_{\|}/\mathscr{R}) - (\partial u_{\|}/\partial n)$. The main drawback of the strong formulation is that the scheme used for the boundary points is not the same as the one used for the interior points. Therefore it violates the global conservation, as will be shown in numerical experiments. Also, the implementation of the strong boundary condition in a cell vertex finite volume framework is straightforward, whereas it is not so in the case of the cell center finite volume framework. This is due to the fact that in the cell center finite volume schemes the reference points of the boundary cells are not coincident with the wall boundary. In fact, in this framework, the normal velocity is not zero at the reference points of the boundary cells and Equation (7a) is not valid. For structured meshes this problem is overcome by introducing half cells on the wall boundary. Therefore it is important to design less dissipative weak boundary conditions which take into account the curvature effects.

3.2. Weak formulation

One of the essential elements of weak wall boundary condition is that the slip condition is enforced only in an integral sense (through the flux function). Consequently, the slip condition $u_{\perp} = 0$ is not satisfied exactly by the state variables on the boundary. Therefore the weak wall boundary condition reduces to determining the fluxes on the cell interfaces coinciding with the wall boundary. It is important to note that the implementation of the weak boundary condition essentially remains the same in both the cell center and cell vertex finite volume frameworks, and that the reference points of the boundary cells are still updated using Equation (1). Here we present three different weak formulations.

3.2.1. Pressure extrapolation method. Using the fact that the fluid velocity normal to the wall is zero, the fluxes on the wall boundary are solely given by Equation (6). One of the ways of obtaining the pressure p_{B} on the wall is to solve the normal momentum equation, as is done while enforcing the strong boundary condition. But this boundary procedure is found to produce an artificial boundary layer [14]. The other way is to extrapolate the pressure from the interior. A zero-order extrapolation requires the use of the pressure at the reference point itself to calculate the wall flux. This procedure is more meaningful in the case of cell vertex framework, where the reference points lie on the wall boundary. When a linear reconstruction procedure is used, the gradient of pressure p in the boundary cell is directly available (if primitive variables are used in the reconstruction procedure) or derivable from other gradients (if conserved/characteristic variables are used in the reconstruction procedure). This information regarding the gradients is used in obtaining the pressures at the Gaussian points on the wall boundary and wall fluxes can be determined using numerical integration procedure.

3.2.2. Mirror condition. In this condition the approximate Riemann solver used to determine the fluxes in the interior edges is also used on the wall boundary. When this procedure is adopted for calculation of fluxes on the wall boundary, information regarding one of the states is obtained from the computational domain (interior state) and the other state (we shall refer to this state as the *fictitious state*) is determined in such a way that the zero normal mass flux across the wall is guaranteed. There are various ways of determining the fictitious state. In this

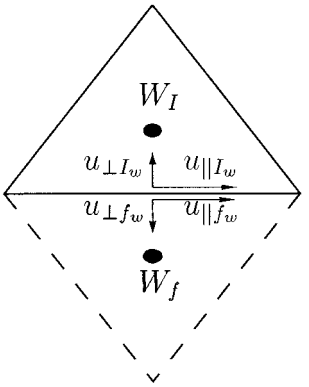

Scheme 2. Mirror boundary condition.

procedure, represented in Scheme 2, the fictitious state velocity vector is obtained by reflecting the velocity vector computed on the wall.

The pressure p_f and the density ρ_f in the fictitious state are assigned the same values as in the interior state. The mirror condition can be represented as

$$u_{\perp f} = -u_{\perp I}, \qquad u_{\| f} = u_{\| I}, \qquad p_f = p_I, \qquad \rho_f = \rho_I, \tag{12}$$

where the subscripts f and I refer to the fictitious state and the state obtained from the computational domain respectively. In Scheme 2 the additional subscript w has been introduced to denote the values at the wall obtained from the reconstruction procedure. The main advantage of the mirror condition is that it permits the use of the interior scheme (an approximate Riemann solver) on the wall boundary and thus it takes into account the direction of information propagation. Its drawback is that it does not take into account the effect of curvature and it is dissipative. For instance, in the cell center framework, in the case of first-order schemes, the variables at the wall ρ_{f_w}, $u_{\perp f_w}$, $u_{\| f_w}$ and p_{f_w} are given by the cell values themselves. Therefore, using this boundary condition assumes zero normal pressure and density gradients on the wall and thus violates the Crocco's relation (7b) and the momentum relation (7d) [15]. When a higher order reconstruction procedure is adopted, though the spatial variation of the variables are properly represented, numerical experiments indicate that this alone is not sufficient to make the boundary condition less dissipative.

The other variation of the mirror condition is presented in Reference [1]. In this procedure $u_{\|}$ is determined using Equation (11) rather than as described in Equation (12), wherever the physics of the fluid flow permits the use of Equation (11). Though this procedure results in improved Mach contours compared with the original mirror condition, it does not significantly improve the wall entropy levels. Therefore, the results obtained using this procedure are not presented in this paper.

3.2.3. Kinetic characteristic boundary condition (KCBC). This procedure is based on the specular reflection model of kinetic theory of gases. This boundary condition is more physical compared with the wall reflection boundary condition described above, in the sense that it does not require fictitious states to be defined on the wall boundary, and at the same time takes into account the direction of information propagation using the specular reflection of molecules at the wall. The following expressions for the wall fluxes obtained following the KCBC procedure are derived in Reference [10]:

$$\mathbf{F}_{\mathrm{B}} = \begin{bmatrix} 0 \\ 2n_x((p_{\mathrm{I}} + \rho_{\mathrm{I}} u_{\perp \mathrm{I}}^2) X_{\mathrm{I}}^+ + \rho_{\mathrm{I}} u_{\perp \mathrm{I}} Y_{\mathrm{I}}) \\ 2n_y((p_{\mathrm{I}} + \rho_{\mathrm{I}} u_{\perp \mathrm{I}}^2) X_{\mathrm{I}}^+ + \rho_{\mathrm{I}} u_{\perp \mathrm{I}} Y_{\mathrm{I}}) \\ 0 \end{bmatrix}, \tag{13}$$

where

$$B_{\mathrm{I}} = u_{\perp \mathrm{I}} \sqrt{\beta}, \qquad X_{\mathrm{I}}^+ = \frac{1 + (erf)(B_{\mathrm{I}})}{2}, \qquad Y_{\mathrm{I}} = \frac{\exp(-B_{\mathrm{I}}^2)}{2\sqrt{\pi\beta}}, \qquad \beta = \frac{\rho}{2p},$$

and

$$erf(x) = \frac{2}{\sqrt{\pi}} \int_0^x \mathrm{e}^{-y^2} \, \mathrm{d}y.$$

3.3. Modified boundary conditions

Apart from the conventional weak formulations discussed above, it is possible to construct modified weak formulations based on certain physical and numerical constraints. We discuss three of such modified formulations here.

3.3.1. Flux equality method. This boundary condition was derived by Deconinck and Struijs [16]. The boundary procedure is similar to the mirror condition, in the sense that it defines a fictitious state to determine the wall fluxes. In this procedure the unknowns along the boundary (the fictitious state) are determined such that the flux calculated using the approximate Riemann solver based on the fictitious state and the interior variables leads to a flux which satisfies the boundary condition (6). If $\mathbf{F}_{\perp \mathrm{B}}$ is the exact boundary flux calculated using the fictitious state and $\tilde{\mathbf{F}}_{\perp \mathrm{B}}$ is the numerical flux function, then the fictitious state is obtained requiring that

$$\tilde{\mathbf{F}}_{\perp}(\mathbf{W}_{\mathrm{I}}, \mathbf{W}_{\mathrm{B}}) = \mathrm{F}_{\perp \mathrm{B}}(\mathbf{W}_{\mathrm{B}}). \tag{14}$$

Equation (14) is a non-linear algebraic relation between interior unknowns $\mathbf{W}_{\mathrm{I}}$ and the boundary unknowns $\mathbf{W}_{\mathrm{B}}$. For the van Leer scheme, solving Equation (14) results in [16]

$$u_{\perp \mathrm{B}} = 0, \qquad u_{\parallel \mathrm{B}} = u_{\parallel \mathrm{I}}, \qquad a_{\mathrm{B}} = a_{\mathrm{I}} \left[1 + \frac{(\gamma - 1)}{2} M_{\mathrm{I}} \right],$$
$$\rho_{\mathrm{B}} = \rho_{\mathrm{I}} (M_{\mathrm{I}} + 1)^2 \left[1 + \frac{(\gamma - 1)}{2} M_{\mathrm{I}} \right]^{-1}. \tag{15}$$

The distinguishing feature of this boundary condition is that for a linear set of equations, it reduces exactly to the characteristic boundary condition. For Euler equations, the direction of information propagation is taken care of by the use of the interior scheme itself. It is interesting to observe that this boundary procedure reduces to the *mirror condition* for M_{I} tending to 0. Also, by using this boundary procedure, it is not possible to obtain a closed form expression for the boundary fluxes for all upwind schemes (consistent with the interior scheme), because of the resulting non-linear algebraic equations.

3.3.2. Modified pressure extrapolation method. Here we present a variation of the pressure extrapolation method described in the previous section. In this variation, we propose that the pressure and density gradients in the boundary cells are no longer determined using Equations (3) or (5), but using the steady state momentum equations and isentropic relation. Therefore, the expressions for the pressure and the density gradients are given by

$$\nabla p = -\rho(\vec{u}\cdot\nabla)\vec{u}, \qquad \nabla\rho = \frac{1}{a^2}\nabla p. \tag{16}$$

In the above expressions, gradients of the velocities are still determined using Equations (3) or (5). It is important to note that the modified gradients of pressure and density are used in the calculation of fluxes for both the interior and the boundary edges of the boundary cell.

3.3.3. Mixed boundary condition. From the above discussion it is clear that while the strong formulation takes into account the curvature effects, the weak formulations, such as the mirror condition, permit the use of the interior scheme itself and thus take care of the direction of information propagation. In order to harness the advantages of both the strong and weak formulations, we propose the following *mixed boundary treatment*.

In this boundary condition we make use of the strong formulation to determine the fictitious state. The interior state is determined in a similar way to the *mirror condition*. This allows the use of an approximate Riemann solver to determine the wall fluxes. As can be easily seen, this boundary treatment is also not conservative since it allows the transpiration of mass flux across a rigid wall. The use of such a boundary condition can be justified by the fact that the computed fluid velocities normal to the wall at steady state are small and therefore the numerical error involved is also small. Numerical results support this fact.

Following an approach similar to the one proposed by Deconinck and Struijs [16] it is possible to correct the zero normal velocity obtained from the strong formulation (to be used in the fictitious state), so that zero mass flux across the rigid wall is satisfied. In this procedure we still compute the variables such as density, pressure and total enthalpy in the fictitious state using the strong formulation. The expression for the corrected normal velocity in the fictitious state for the van Leer scheme is

$$u_{\perp \mathrm{f_w}} = a_{\mathrm{f_w}} - (u_{\perp \mathrm{I_w}} + a_{\mathrm{I_w}})\left(\frac{\rho_{\mathrm{I_w}} a_{\mathrm{f_w}}}{\rho_{\mathrm{f_w}} a_{\mathrm{I_w}}}\right)^{1/2}. \tag{17}$$

Interestingly, the use of the above relation for determining $u_{\perp \mathrm{f_w}}$ also satisfies the zero energy flux across the wall for the van Leer flux corrected by Hänel, which preserves total enthalpy in the entire flow field. Contrary to the expectations, the numerical experiments indicate that this modification is sensitive to the asymmetry in the grid, a feature similar to the strong boundary conditions. Therefore, the results are not presented for this case in the following section.

4. NUMERICAL EXPERIMENTS

The boundary conditions discussed in the previous section are tested for various schemes for the following test cases:

(i) Symmetric transonic flow past NACA 0012.
(ii) Subsonic flow past NACA 0012.
(iii) Supersonic flow past a semi cylinder.
(iv) Hypersonic flow past double ellipse

The details regarding the grids used for the different computations are presented in Table I. Grid 1 is a symmetric regular triangular grid and grids 2–4 are asymmetric unstructured grids. The fine grid, grid 3, has been generated by adding a node at the midpoint of the edges of the coarse grid (grid 2) and recovering four triangles from each of the coarse grid triangles. Thus

Table I. Grid details

Name	Configuration	Nodes	Cells	Edges
Grid 1	Airfoil NACA 0012	3200	6144	9344
Grid 2	Airfoil NACA 0012	2779	5438	8217
Grid 3	Airfoil NACA 0012	10 996	21 752	32 748
Grid 4	Half cylinder	3870	7456	11 325
Grid 5	Double ellipse	6844	13 325	20 168

grid 3 preserves the asymmetry of the parent grid. Grid 5 is a regular triangular grid, adapted in the cabin shock region.

In the results presented, the wall entropy deviation is defined as $\Sigma = (p/p^{\infty})(\rho^{\infty}/\rho)^{\gamma} - 1$. The discussions on the effect of the boundary condition presented in the following sections are generally found to be independent of the interior scheme used.

4.1. Transonic flow past NACA 0012

The computations are made for a free stream Mach number of 0.85 and 0° angle of attack. This symmetric transonic flow is an interesting test case, because the unstructured meshes generated around airfoils, by definition, need not be symmetric and the use of non-conservative boundary treatment in computing flows with shocks can introduce asymmetry in the flow, which otherwise should be symmetric. A good boundary condition is expected to be insensitive to this grid-induced asymmetry. In the following computations on unstructured meshes, the flow is understood to be symmetric if both the upper and lower shocks share the corresponding locations on the top and bottom walls, respectively.

4.1.1. Coarse grid results. The symmetric regular triangular grid (grid 1) and asymmetric unstructured grid (grid 2) used in the computation are presented in Figure 1. The Mach contours and the wall entropy levels for this test case with strong boundary condition are presented in Figure 2. The asymmetry in the solution obtained using grid 2, indicates that the strong boundary conditions are sensitive to the grid-induced asymmetry. The figures also indicate that the strong boundary formulation is sensitive to the way the normal momentum equation is satisfied.

The results obtained using different weak boundary formulations are presented in Figures 3 and 4. One of the important features of the results obtained using the weak formulations is

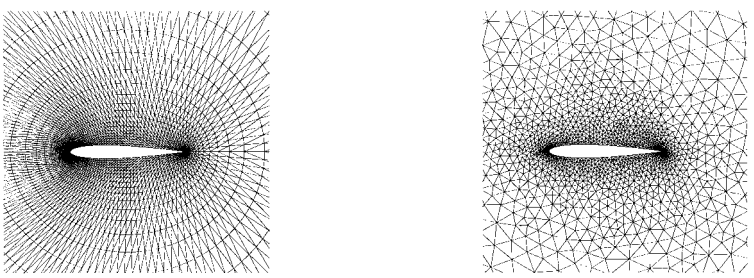

Grid 1 Grid 2

Figure 1. Symmetric and asymmetric grids used in the calculations.

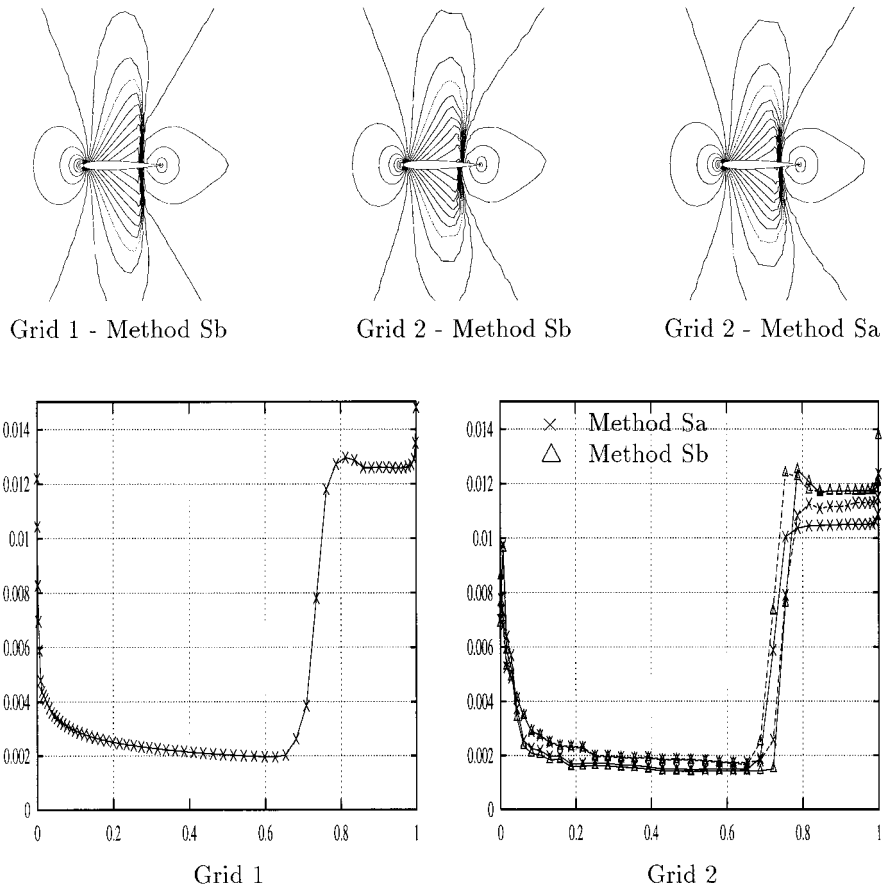

Figure 2. Strong boundary condition—Mach contours and wall entropy Roe scheme—cell vertex finite volume. Flow past NACA 0012 $M_\infty = 0.85$, angle of attack = 0° (— top wall, --- bottom wall).

that they all preserve the symmetry of the flow. The results obtained using the mirror condition, KCBC and flux equality method show non-physical curvature of the Mach contours on the wall. This feature is less pronounced in the case of pressure extrapolation boundary conditions. The mixed boundary condition preserves symmetry and at the same time the quality of the Mach contours are comparable with those obtained using the strong boundary condition.

The observations that have been made based on the Mach contours presented in Figure 3 can be re-emphasised using the entropy levels presented in Figure 4. From Figure 4 it is clear that the best entropy levels are obtained using the mixed boundary condition. It can also be seen that the modified pressure extrapolation method produces better entropy levels compared with the pressure extrapolation method. The entropy levels obtained using all the rest of the weak formulations are an order of magnitude higher than the entropy levels obtained using the mixed boundary treatment.

The lift and drag coefficients computed using different boundary procedures are presented in Table II. The lift coefficient predicted for this zero lift case is a measure of asymmetry in the solution. The asymmetry of the solutions obtained using the strong boundary conditions

manifests in the form of relatively higher lift coefficients and underprediction of the wave drag. The best prediction of the lift coefficient is by the mixed boundary condition.

It is found that mixed boundary treatment produces improved results, even in the case of cell center finite volume schemes. A comparison of the results obtained using the cell center finite volume schemes is found in Reference [17].

4.1.2. Fine grid results. Here we summarize some quantitative results using a finer grid (grid 3). We restrict our attention to the numerical boundary conditions which lead to better results. The entropy deviations are plotted in Figure 5. In Table III we present theoretical and computed entropy jumps across the shock on the top wall of the airfoil. The theoretical entropy jumps are computed using the normal shock relation, based on the upstream Mach number (which is the maximum Mach number reached on the top wall). We observe that using the strong formulation *Sa* still leads to asymmetric results on this finer grid. Though the results obtained using the strong formulation *Sb* remain symmetric, the jump predicted is inaccurate. The jumps predicted using both the mixed and the pressure extrapolation boundary conditions are accurate.

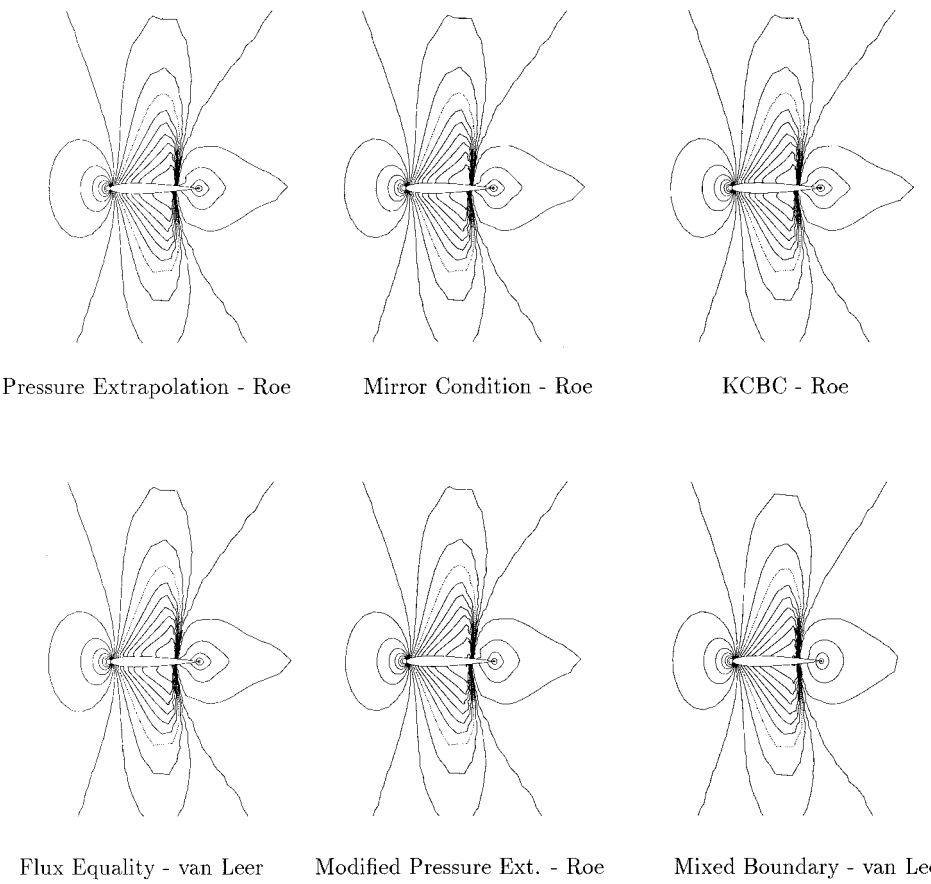

Figure 3. Mach contours obtained using weak boundary condition cell vertex finite volume. Flow past NACA 0012 $M_\infty = 0.85$, angle of attack = 0°, grid 2.

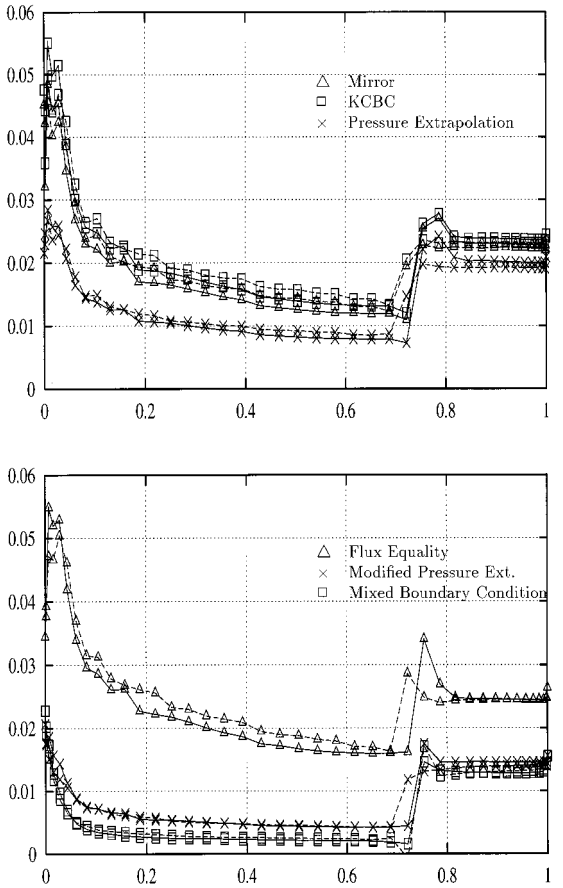

Figure 4. Wall entropy obtained using cell vertex finite volume scheme. Flow past NACA 0012, $M_\infty = 0.85$, angle of attack = 0°, grid 2 (— top wall, --- bottom).

4.2. Subsonic flow past NACA 0012

Here the computations are made for a free stream Mach number of 0.63 and 2° angle of attack (zero drag case). In this test case entropy layer generated because of the wall boundary condition becomes more apparent when we look at the Mach contours presented in Figure 6.

Table II. Flow past NACA 0012 airfoil, $M_\infty = 0.85$, $\alpha = 0°$

Boundary condition	Lift coefficient	Drag coefficient
Strong *Sa*	−0.0252	0.0413
Strong *Sb*	0.0352	0.0405
Mirror	0.0190	0.0450
KCBC	0.0185	0.0447
Pressure extrapolation	0.0196	0.0473
Modified pressure extrapolation	0.0209	0.0474
Flux equality method	0.0194	0.0439
Mixed	−0.0063	0.0451

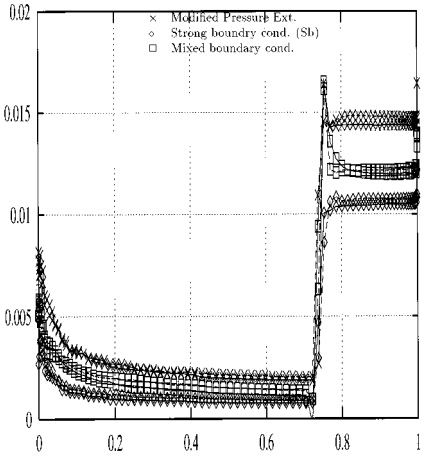

Figure 5. Wall entropy obtained using cell vertex finite volume scheme. Flow past NACA 0012, $M_\infty = 0.85$, angle of attack = 0°, grid 3 (— top wall, --- bottom wall).

The contours obtained using the strong boundary condition and the mixed boundary condition are of superior quality. The contours obtained using the modified pressure extrapolation boundary condition are better than those obtained using mirror condition, KCBC or flux equality method. Similar to the previous test case the above mentioned observations can be re-emphasised looking at the wall entropy deviation presented in Figure 7.

At this point, it is worthwhile to make some remarks on the use of the Crocco relation (7b) which involves the computation of vorticity on the wall. In Figure 8 we present the wall vorticities obtained using the mixed boundary condition, both for transonic and subsonic test cases. From the figure it is clear that even if the flow is irrotational (as in the subsonic test case) or permits only small entropy gradient (as in the transonic test case), the vorticities computed on the wall are considerably high because of the numerical errors. This problem is found to be more acute in the stagnation regions and is accentuated with the use of limiters. In fact, the use of such erroneous wall vorticity values in satisfying the entropy condition on the wall makes the boundary condition more dissipative. All the computations presented in this work are obtained using second-order schemes. Possibly, use of third-order schemes, coupled with sufficiently finer meshes and higher order methods to estimate the values of the vorticity itself, will help overcome this problem. Nevertheless, the use of the Crocco relation is very important in extending the applicability of the strong and mixed boundary conditions discussed in this paper, to flows which do not satisfy the zero normal entropy gradient on the wall. From various numerical experiments performed, it was found that the mixed boundary condition suggested in this work is found to be more robust compared with the strong boundary condition, when used in conjunction with the Crocco relation. Further research in this direction is underway.

Table III. Comparison of entropy jumps on fine grid

Boundary method	M_{maximum}	$\Delta\Sigma_{\text{Theoretical}}$	$\Delta\Sigma_{\text{Computed}}$	Relative error (%)
Strong *Sb*	1.355	0.0128	0.0098	23
Modified pressure extrapolation	1.349	0.0123	0.0126	2
Mixed	1.357	0.0130	0.0119	8

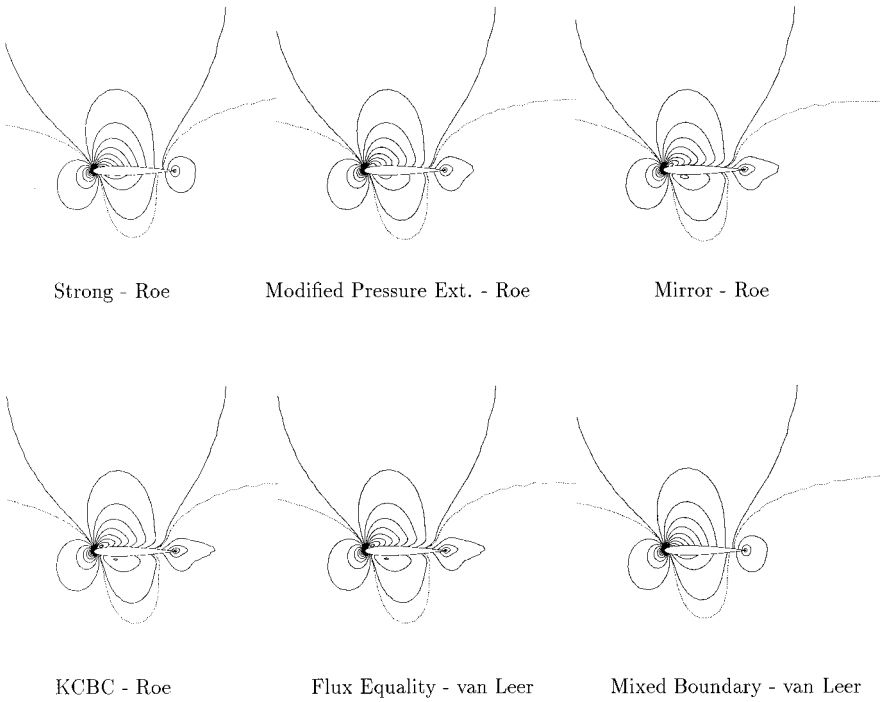

Figure 6. Mach contours obtained using weak boundary condition cell vertex finite volume. Flow past NACA 0012 $M_\infty = 0.63$, angle of attack $= 0°$, grid 2.

4.3. Supersonic flows

4.3.1. Flow past a semi cylinder. Here comparisons are made for the free stream Mach number $M_\infty = 4$. All computations were performed using a KFVS cell vertex scheme with a minmod limiter. Despite uniform inflow conditions, vorticity is generated through the strong bow shock standing upstream of the cylinder. Nevertheless on the body streamline the vorticity is zero due to the symmetry of the problem. The results presented for the strong boundary condition assume zero vorticity on the wall (*Method Sc*).

An asymmetric adapted grid (grid 4) shown in Figure 9(a) was used. Mach number contours and entropy contours obtained using the mixed boundary condition are plotted in Figure 9(b,c), respectively. The comparisons are made for the wall entropy deviations and the wall vorticities plotted in Figure 9(d,e).

The strong formulation does not lead to as good results as in the case of subsonic or transonic flow calculations. The convergence history for an explicit scheme is presented in Figure 9(f). The mixed boundary condition again seems to be the best compromise in terms of accuracy and robustness.

4.3.2. Flow past double ellipse. The calculations for this test case have been made for a free stream Mach number of 8.15 and 30° angle of attack. The grid used in this computation (grid 5) is presented in Figure 10(a). Apart from the bow shock standing upstream to the body, the flow is also characterised by a cabin shock. Interestingly, the cabin shock is a detached shock and should satisfy the normal shock relation on the wall. This is an interesting test case, because the normal gradient of entropy on the wall is not zero, as is evident from the entropy

contours presented in Figure 10(d). The Mach contours obtained using the mixed boundary procedure wherein the Crocco relation is used to define the entropy gradient on the wall, and the one where the zero normal entropy gradient is assumed, are presented in Figure 10(b,c). Both of the above mentioned procedures produce identical results, except near the wall. While the Mach contours obtained using the strong boundary formulation are identical to those obtained using the mixed boundary condition with zero normal entropy gradient, those obtained using the simple pressure extrapolation method resemble the other case presented here. Clearly, as discussed in the airfoil test case, we see that the use of computed vorticity in satisfying the entropy gradient on the wall, makes the boundary condition more dissipative. The wall Mach and entropy values presented in Figure 10(e,f) also re-emphasise the above statement. Interestingly, the assumption of zero normal entropy gradient on the wall (both for the strong and mixed boundary conditions) seem to produce good results even in this hypersonic test case. This needs further investigation.

5. CONCLUSIONS

A comparison of various methods of implementing the wall boundary conditions have been discussed. From the discussions presented in the previous pages the following conclusions can be drawn.

The mixed boundary condition, which has the advantages of both strong and weak formulations has been suggested. This boundary condition permits the use of any approximate Riemann solver on the wall and is found to drastically improve the solution when used in conjunction with flux vector splitting schemes. Unlike the strong boundary procedure this boundary condition is less sensitive to grid-induced asymmetry and to the way the normal

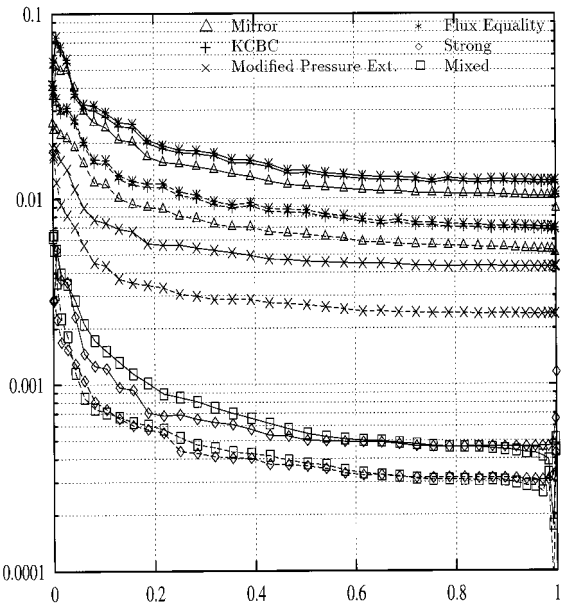

Figure 7. Wall entropy obtained using cell vertex finite volume scheme. Flow past NACA 0012, $M_\infty = 0.63$, angle of attack = 2°, grid 2 (— top wall, --- bottom wall).

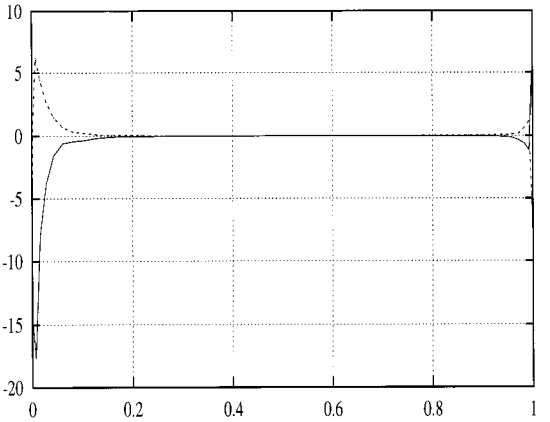

(a) $M_\infty = 0.63$, $\alpha = 2.0°$

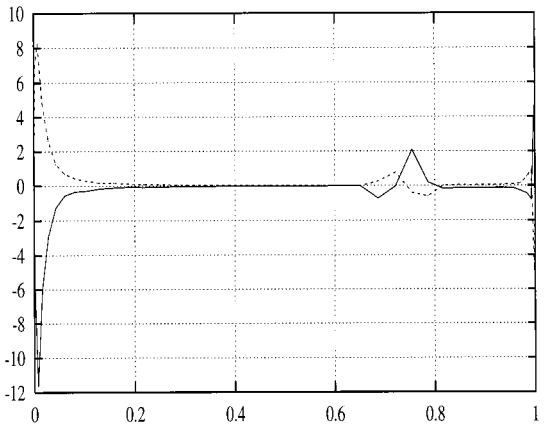

(b) $M_\infty = 0.85$, $\alpha = 0.0°$

Figure 8. Wall vorticity obtained using the mixed boundary condition. Flow past NACA 0012, grid 2 (— top wall, --- bottom wall).

momentum equation is satisfied on the wall. It has also been demonstrated that this boundary procedure can be implemented with equal ease both in cell center and cell vertex frameworks. The mixed boundary condition with a zero normal entropy gradient produces good results for all the flow regimes. But, its use in conjunction with the Crocco relation needs to be investigated further.

The modified pressure extrapolation method (b) wherein the pressure and density gradients on the boundary cells are corrected using certain physical constraints, inspired by the strong formulation, is also very promising for transonic flow computations.

The other weak formulations namely the mirror, KCBC and flux equality method are found to be dissipative and fine grid computation does not seem to improve the quality of the results. Among all the dissipative weak formulations, the KCBC is more physical and it remains to be explored if the experience gained in using the strong formulation can be adopted for improving this kinetic boundary condition.

The results obtained using both strong and weak formulations indicate that the solutions are not sensitive to the way the gradients are determined in the cells. Nevertheless, Equations (3) and (5) are useful in satisfying the gradient boundary conditions on the wall.

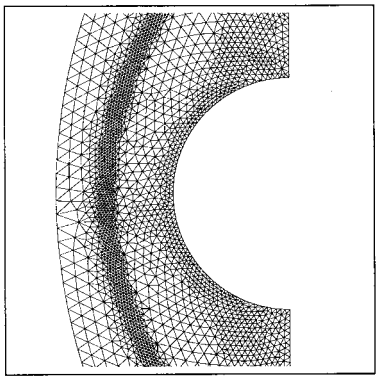

(a) half − cylinder : 3870 points
7456 triangles
11325 edges

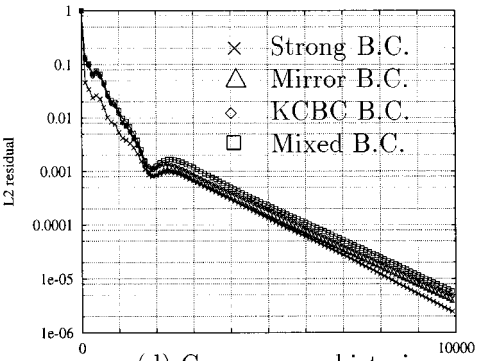

(d) Convergence histories

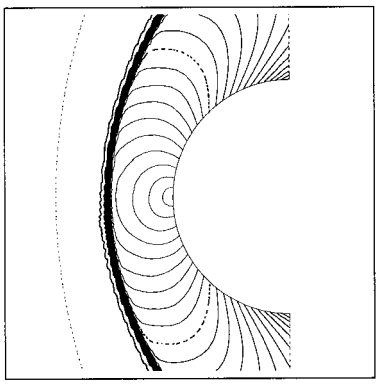

(b) Mach number contours
$min = 0.1,\ max = 4.0$
$\Delta = 0.1$, dotline $= 1.0$

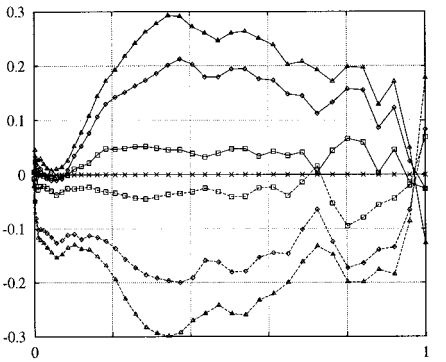

(e) Wall vorticities

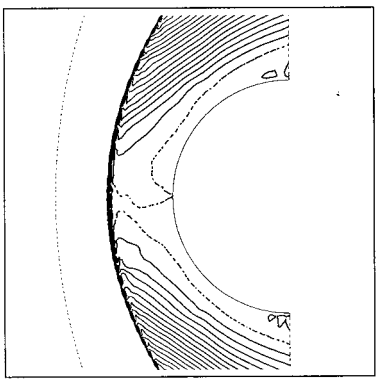

(c) Entropy contours
$min = 0.71,\ max = 1.31$
$\Delta = 0.02$, dotline $= 1.21$

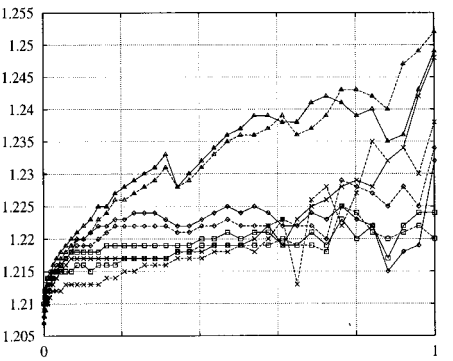

(f) Wall Entropy deviations

Figure 9. Flow past a half cylinder, $M_\infty = 4$. KFVS scheme using *minmod* limiter.

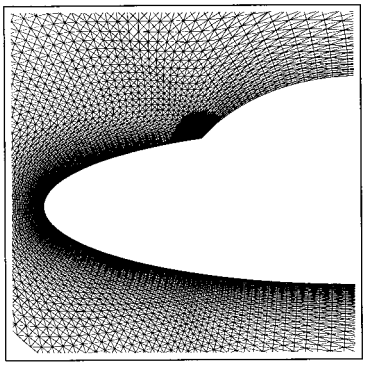

(*a*) Double ellipse

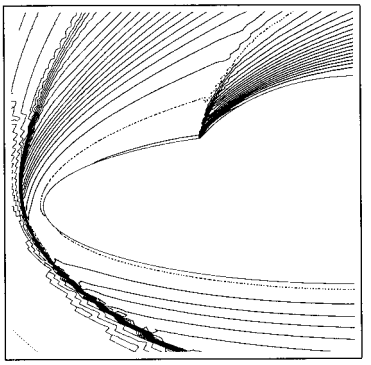

(*d*) Entropy contours
$min = 0.0,\ max = 12.0$
$\Delta = 0.3, \text{dotline} = 6.0$

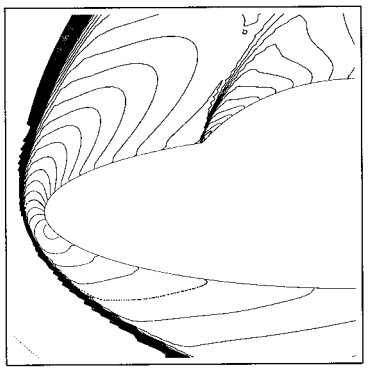

(*b*) Mach number contours
Mixed B. C. with Crocco
$min = 0.0,\ max = 8.0$
$\Delta = 0.2$, dotline = 1.0

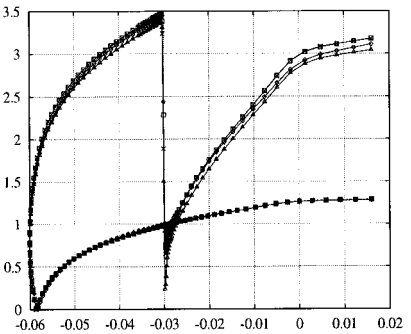

(*e*) Wall Mach numbers
× Strong B.C.
△ Pressure Extrapolation
◇ Mixed with Crocco
□ Mixed without Crocco

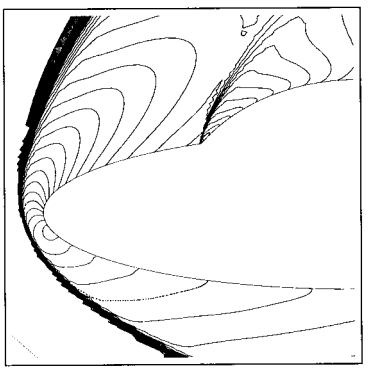

(*c*) Mach number contours
Mixed without Crocco

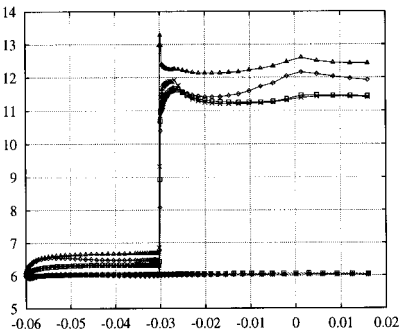

(*f*) Wall Entropy deviations
Mixed without Crocco

Figure 10. Flow past a double ellipse, $M_\infty = 8.15$, $\alpha = 30°$. KFVS scheme using *Venkatakrishnan* limiter.

In the stagnation region the gradients in the flow field are high and this results in increased numerical error. This is true for all types of boundary conditions. The use of finer mesh (in the regions of higher gradient) and schemes of higher order accuracy are expected to solve this problem. Also, the transonic calculations on unstructured meshes are found to be sensitive to the limiting procedures used and frequently switching off the limiters on the boundary cells improve the values obtained on the wall, particularly in the stagnation region.

As indicated earlier, a conservative boundary treatment is very important for the accurate solution of the conservation laws which permit discontinuous solution. Therefore future efforts should be directed towards building wall boundary conditions which are genuinely conservative and at the same time take care of the curvature effects.

ACKNOWLEDGMENTS

The authors would like to thank Professor A. Lerat and Dr. V. Daru, for their useful comments and encouragement during the course of this work.

APPENDIX A. APPROXIMATE RIEMANN SOLVERS

- Roe flux function [8]: the flux function reads:

$$\tilde{\mathbf{F}}_{\perp}^{\mathrm{Roe}}(W_R, W_L) = \tfrac{1}{2}(\mathbf{F}_{\perp}(W_R) + \mathbf{F}_{\perp}(W_L)) - \tfrac{1}{2}|\mathscr{A}(W_R, W_L, \hat{n})|(W_R - W_L),$$

  where $\mathscr{A}(W_R, W_L, \hat{n})$ is the Jacobian matrix defined using Roe's average:

$$\langle \rho \rangle = \frac{\sqrt{\rho_L}\rho_R + \sqrt{\rho_R}\rho_L}{\sqrt{\rho_R} + \sqrt{\rho_L}}, \qquad \langle \vec{u} \rangle = \frac{\sqrt{\rho_R}\vec{u}_R + \sqrt{\rho_L}\vec{u}_L}{\sqrt{\rho_R} + \sqrt{\rho_L}},$$
$$\langle H \rangle = \frac{\sqrt{\rho_L}H_R + \sqrt{\rho_R}H_L}{\sqrt{\rho_R} + \sqrt{\rho_L}}.$$

- Van Leer flux function [9]: the flux function is written as

$$\tilde{\mathbf{F}}_{\perp}^{\mathrm{Leer}}(W_R, W_L) = \mathbf{F}_{\perp}^{+}(W_R) + \mathbf{F}_{\perp}^{-}(W_L).$$

  With the local algebraic Mach number $M_{\perp} = u_{\perp}/a$ components read

$$\tilde{\mathbf{F}}_{\perp}^{\pm} = \pm\frac{\rho a}{4}(M_{\perp} \pm)^2 \begin{bmatrix} 1 \\ n_x[(\gamma-1)u_{\perp} \pm 2a]/\gamma - n_y u_{\parallel} \\ n_y[(\gamma-1)u_{\perp} \pm 2a]/\gamma - n_x u_{\parallel} \\ \frac{1}{2}\left(\frac{[(\gamma-1)u_{\perp} \pm 2a]^2}{\gamma^2-1} + u_{\parallel}^2\right) \end{bmatrix}.$$

  Hänel's correction corresponds to $F_4^{\pm} = F_1^{\pm} H$.

- Kinetic flux function [10]: the flux components read

$$\tilde{\mathbf{F}}_{\perp}^{\pm} = \begin{bmatrix} \rho u_{\perp} X^{\pm} \pm \rho Y \\ n_x(p + \rho u_{\perp}^2) X^{\pm} \pm \rho u_{\perp} Y - n_y \rho (u_{\perp} u_{\parallel} X^{\pm} \pm u_{\parallel} Y) \\ n_y(p + \rho u_{\perp}^2) X^{\pm} \pm \rho u_{\perp} Y - n_x \rho (u_{\perp} u_{\parallel} X^{\pm} \pm u_{\parallel} Y) \\ \left[\frac{\gamma}{\gamma - 1} p + \frac{1}{2} \rho (u_{\perp}^2 + u_{\parallel}^2)\right] u_{\perp} X^{\pm} \pm \left[\frac{\gamma + 1}{2(\gamma - 1)} p + \frac{1}{2} \rho (u_{\perp}^2 + u_{\parallel}^2)\right] Y \end{bmatrix},$$

where

$$X^{\pm} = \frac{1 \pm erf(S_n)}{2}, \qquad Y = \frac{\exp(-S_n^2)}{2\sqrt{\pi\beta}}, \qquad Sn = u_{\perp}\sqrt{\beta}, \qquad \beta = \frac{\rho}{2p},$$

$$erf(x) = \frac{2}{\sqrt{\pi}} \int_0^x \mathrm{e}^{-y^2}\, \mathrm{d}y.$$

REFERENCES

1. C. Hirsch, *Numerical Computation of Internal and External Flows*, Wiley, New York, 1991.
2. A.S. Sens and G.D. Mortchelewicz, 'Implicit schemes for unsteady Euler equations on triangular meshes', *Int. J. Numer. Methods Fluids*, **18**, 647–668 (1994).
3. A.K. Ghosh and S.M. Deshpande, 'Least squares kinetic upwind method for inviscid compressible flows', *AIAA-95-1735-CP*.
4. T.J. Barth and P.O. Frederickson, 'Higher order solution of Euler equations on unstructured grids using quadratic reconstruction', *AIAA-90-0013*.
5. F. Fezoui and B. Stoufflet, 'A class of implicit upwind scheme for Euler simulation with unstructured meshes', *J. Comput. Phys.*, **84**, 174–206 (1989).
6. B. van Leer, 'Towards the ultimate conservative difference scheme IV. A new approach to numerical convection', *Lecture notes in Physics*, **23**, 276 (1977).
7. N. Balakrishnan and S.M. Deshpande, 'Reconstruction on unstructured meshes with upwind solvers', *Proc. First Asian CFD Conference*, Jan. 16–19, Hong Kong, 1995.
8. P.L. Roe, 'Approximate Riemann solvers, parameter vectors and difference schemes', *J.C.P.*, **43** (1981).
9. B. van Leer, 'Flux vector splitting for Euler equations', *Lecture Notes in Physics*, **170**, 405–512 (1982).
10. J.C. Mandal and S.M. Deshpande, 'Kinetic flux vector splitting for Euler equations', *Comput. Fluids.*, **23**, 447–478 (1994).
11. V. Venkatakrishnan, 'Convergence to steady state solutions of the Euler equations on unstructured grids with limiters', *J. Comput. Phys.*, **118**, 120 (1995).
12. H.W. Liepmann and A. Roshko, *Elements of Gas Dynamics*, Wiley, New York, 1957.
13. A. Lerat and J. Sides, 'Efficient solution of the steady Euler equations with a centered implicit method', in K.W. Morton and M.J. Baines (eds.), *Numerical Methods for Fluid Dynamics*, Clarendon Press, Oxford, 1988, pp. 65–86.
14. A. Rizzi, 'Numerical implementation of solid-body boundary conditions for Euler equations', *Z.A.M.M.*, **58**, T301–T304 (1978).
15. G. Moretti, 'Importance of boundary conditions in the numerical treatment of hyperbolic equations', *Proc. Int. Symp. High Speed Computing in Fluid Dynamics*, Monterey, 1968.
16. H. Deconinck and R. Struijs, 'Consistent boundary conditions for cell centered upwind finite volume Euler solvers', *Num. Methods Dyn. III*, Clarendon Press, Oxford 12/CFD, April 1988.
17. G. Fernandez and N. Balakrishnan, 'On the use of Crocco relation for wall boundary conditions', *Accepted for presentation in the First International symposium on Finite Volumes for Complex Applications—Problems and Prespectives*, Rouen, France, July 1996.
18. V. Venkatakrishnan, 'A perspective on unstructured grid flow solvers', *ICASE Report # 95-3*, February 1995.

